J. Fluid Mech. (1997), *vol.* 342, *pp.* 119–139. Printed in the United Kingdom

© 1997 Cambridge University Press

Sinusoidal forcing of a turbulent separation bubble

By M. KIYA, M. SHIMIZU AND O. MOCHIZUKI
Department of Mechanical Engineering, Hokkaido University, Sapporo, 060 Japan

(Received 24 November 1995 and in revised form 4 February 1997)

A turbulent separation bubble is forced by single- and double-frequency sinusoidal disturbances, with the emphasis placed on the reattachment length as a function of the forcing amplitude and frequency. The separation bubble is that formed along the side of a blunt circular cylinder with a square leading edge. In single-frequency forcing, the reattachment length attains a minimum at a particular forcing frequency, F, which scales with the frequency of shedding of vortices from the reattachment region of the separated shear layer. A flow model is presented to interpret the frequency F. Forcing of sufficiently high amplitude eliminates the recirculating region in a range of the forcing frequency. Flow visualization and a survey of the mean flow and turbulence properties demonstrate how the flow in the separated shear layer is modified by the forcing. In double-frequency forcing, the superposition of the F-component on its higher or subharmonic components is considered. A non-resonant combination of the two frequencies is also considered.

1. Introduction

The separation of flow from a solid surface is encountered in a number of flow configurations such as aerofoils at high angles of attack, turbomachinery cascades at off-design flow rate, sudden expansions in flow passages, dump combustors, cars and trains, buildings and structures subjected to winds, etc. Separated flows are highly turbulent and unsteady owing to the evolution of vortices in the separated shear layer. The separation of flow in turbomachinery, for example, produces the unfavourable flow unsteadiness, noise, and loss in efficiency. On the other hand, a high level of turbulence associated with separated flows enhances heat and mass transfer, and mixing; this property is favourable for combustors and heat exchangers. However, the separation of flow should be avoided in most engineering applications. When it is unavoidable, the separated region should be reduced as much as possible. This is the reason why control of flow separation and separated flows has been studied for many years, as extensively reviewed by Gad-el-Hak & Bushnell (1991).

Separated flows can be classified into two categories: separated flow with reattachment and without reattachment. A typical example of separated flow with reattachment is the flow around a backward-facing step, while an example of separated flow without reattachment is the flow around a circular cylinder. The former is characterized by the interaction between the separated shear layer and the nearby solid surface, while the latter is characterized by the interaction between two shear layers emanating from the separation lines.

The purpose of the work described in this paper is to study sinusoidal forcing of a separated flow with reattachment, which will be referred to as a separation bubble, with the purpose of obtaining information on active control of separated flows. The separation bubble downstream of the square leading edge of a blunt cylinder whose

https://doi.org/10.1017/S0022112097005521 Published online by Cambridge University Press

axis is aligned with the main flow is chosen here as a simple case. This flow includes no end effects, which are unavoidable in its two-dimensional version, namely the separation bubble downstream of the square leading edge of a blunt plate. Moreover, these two separation bubbles without artificial forcing have basically similar properties as discussed by Kiya (1989) and Sigurdson (1995).

Most of the essential properties of the forced separation bubble have been discussed by Sigurdson (1995) and Sigurdson & Roshko (1988). They have measured the pressure drag acting on the front face of the cylinder as a function of forcing amplitude and frequency, showing that the drag attains a broad minimum at a particular forcing frequency, which will be referred to as the most effective frequency, for a fixed value of the forcing amplitude. They suggest that the minimum occurs when the initial separated shear layer is used to amplify the forcing, creating structures that amalgamate to form a final structure with the frequency of the shedding-type instability f_v. This frequency is irrelevant compared to the initial Kelvin–Helmholtz frequencies at high Reynolds numbers. The mechanism which determines the most effective frequency is the shedding-type instability. Sigurdson and Roshko argue that the shedding-type instability is similar to the instability which leads to the periodic vortex shedding from two-dimensional bluff bodies, being also true for separation bubbles downstream of a backward-facing step and the square leading edge of a blunt plate, and for separated flows around aerofoils. The most effective frequency is found to be 2 to 5 times the shedding frequency f_v.

In the present paper, the reattachment length of the separation bubble is employed as a measure of the effectiveness of sinusoidal forcing. Sigurdson (1995) has been concerned mostly with the drag of the front face, concluding that the drag responds to the forcing frequency in a basically similar manner to the reattachment length. In this paper a flow model is presented to explain the most effective frequency in terms of the frequency of the shedding-type instability f_v. This model supplements Sigurdson's (1995) discussion on the most effective frequency. Furthermore, double-frequency forcing is studied in this paper. Preliminary results of this investigation were reported by Kiya *et al.* (1993, 1995), and Shimizu *et al.* (1993).

Sigurdson's (1995) paper includes an extensive list of references on forced separation bubbles, which interested readers should consult. Here mention will be made of investigations on the forcing of simple separation bubbles other than those mentioned above: flows downstream of a backward-facing step (Bhattacharjee, Scheelke & Troutt, 1986; Roos & Kegelman 1986, 1987), the square leading edge of a blunt plate (Parker & Welsh 1983; Cooper, Sheridan & Flood 1986; Stokes & Welsh 1986) and a sharp-edged inlet to a pipe (Sutton *et al.* 1981), and separated flows around aerofoils (Zaman, Bar-Sever & Mangalam 1987; Huang, Maestrello & Bryant 1987; Bar-Sever 1989; Nishioka, Arai & Yoshida 1990). Roos & Kegelman (1987) have shown that the reattachment length attains a minimum at a forcing frequency which depends weakly on the forcing amplitude.

The flow configuration is shown in figure 1. A blunt circular cylinder of diameter d is placed in the main flow of velocity U_∞. The cylindrical coordinates $x, r,$ are employed, where x is the longitudinal distance along the axis of the cylinder, r is the radial distance, and is the azimuthal angle about the axis $x = 0$; the origin is at the centre of the front face of the cylinder. The boundary layer separated from the square leading edge reattaches, in terms of the time-mean flow, onto the surface of the cylinder to generate the separation bubble. The x-coordinate of the reattachment position is denoted by x_R; the distance between the separation edge and the reattachment position is referred to as the reattachment length.

https://doi.org/10.1017/S0022112097005521 Published online by Cambridge University Press

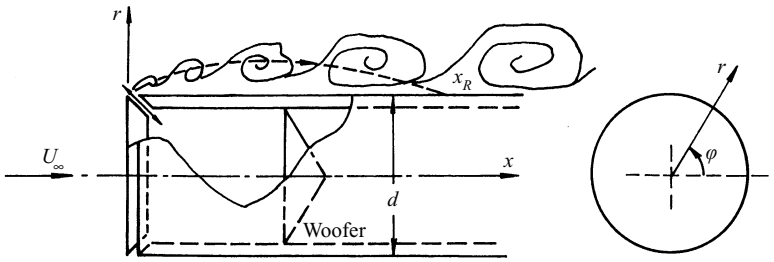


FIGURE 1. Cross-sectional view of the blunt circular cylinder and definition of the coordinate system. The inclined double-ended arrow indicates oscillating flow in the slot produced by the woofer.

The arrangement of the paper is as follows. In §2 experimental apparatus and methods are described. Results for the single-frequency forcing are presented in §3, and those for the double-frequency forcing are presented in §4. The results are discussed in §5. Finally, §6 is the conclusion.

2. Experimental apparatus and method

2.1. *Wind tunnel, circular cylinder, and data acquisition*

The experiments were performed in a closed-return wind tunnel with a 1.5 m wide, 1.2 m high and 6.0 m long working section. The ceiling of the working section was shaped so as to realize a negligibly small longitudinal presure gradient. The free-stream turbulence intensity was 0.2–0.3 % at speeds of 5–20 m s^{-1}. The acoustic pressure level measured near an air breather at the end of the working section was 0.5–1.2 Pa in the same range of speed. No significant peaks were found in the spectrum of the velocity fluctuations in the main flow or that of the acoustic pressure.

A blunt circular cylinder with diameter $d = 0.200$ m and length of 2.00 m was used in the experiment. The cylinder was constructed from Plexiglas, consisting of a front disc 1.0 cm in thickness and a circular pipe 0.5 cm in thickness (figure 1). The front disk was bevelled by 45° towards the downstream side to form a knife edge, being set in position by a screw device. The upstream end of the circular pipe was bevelled by 45° in a manner shown in figure 1, so that a slot was formed between the front disc and the circular pipe. The width of the slot was set equal to 2.75 ± 0.05 mm, where the error is the r.m.s. deviation in the azimuthal direction. The length of the cylinder is more than 6 times the reattachment length of the unforced separation bubble (see §3.1), so that an unsteady separated flow downstream of the blunt trailing edge of the cylinder is assumed to have negligible effects on the flow in the leading-edge separation bubble.

A woofer was installed inside the cylinder as shown in figure 1; this was driven by a power amplifier with a sinusoidal output of controllable frequency and amplitude to introduce a sinusoidal velocity disturbance into the separated shear layer. For the double-frequency forcing, a signal synthesizer was used to produce two sinusoidal outputs of different frequencies and amplitudes with an arbitrary phase difference. The two sinusoidal outputs were added and then supplied to the power amplifier. The amplitude of the velocity fluctuation measured, with the main flow off, at the centre of the slot by an I-type hot-wire probe was uniform within ± 18 % and ± 2 % at the forcing frequencies of 20 Hz and 100 Hz, respectively.

The cylinder was installed into the working section along its central axis, being set

https://doi.org/10.1017/S0022112097005521 Published online by Cambridge University Press

in position by four piano wires 0.9 mm in diameter at three longitudinal stations $x/d = 2.3$, 7.0 and 9.5. Vibration of the piano wires due to the periodic vortex shedding was prevented by attaching flags of a thin scotch tape at a number of different positions of the wires. The exact alignment of the cylinder was found by matching time-mean pressures recorded on four pressure tappings located along the circumference with an angle of 90° at the station $x/d = 2.0$. The time-mean and r.m.s. velocities in the unforced separation bubble were sufficiently axisymmetric (Kiya *et al.* 1991). The axisymmetry of the forced flow was demonstrated by a surface-flow visualization using tuft probes.

The blockage of the cylinder was only 1.7%. Thus no attempt was made to correct the blockage effect.

A single I-type hot-wire probe and a split-film probe (Thermo-Systems Inc. Model 1288) were used to measure the time-mean and fluctuating velocities. The hot-wire probe was set normal to the (x, r)-plane, so that this probe measured the velocity component in the same plane, say $q^* = Q + q$, where Q and q are the time-mean and fluctuating components. The split-film probe was also set normal to the (x, r)-plane with its plane of split normal to the main-flow direction. Thus this probe detected the intermittent reversal of the local-flow direction, being used to obtain the reverse-flow intermittency near the surface. Each probe was mounted on a traversing mechanism inside the test section.

Data acquisition was by the use of a personal computer, which also controlled the traverse of the probes. The data were AD-converted and stored on a magnetic disc, being analysed later on the computer and on a real-time signal processor.

Flow visualization was by a smoke wire, and by tuft probes distributed on the surface of the cylinder. The smoke wire was situated near the surface, parallel to the x-axis.

The experiments were performed in the range of Reynolds number $Re \equiv U_\infty d/\nu = (0.69\text{–}2.76) \times 10^5$, which approximately corresponded to the main-flow velocity $U_\infty = 5.0\text{–}20.0$ m s^{-1}. The flow visualized by smoke was at the lower Reynolds number $Re = 1.4 \times 10^4$.

2.2. *Definition of forcing amplitude*

The amplitude of a sinusoidal velocity disturbance generated by the forcing was defined at a position near the separation edge in the presence of the main flow. For the determination of this 'reference' position, the velocities Q and q' (which is the r.m.s. value of q) were measured in the unforced flow along a longitudinal line at $r = d/2$ upstream of the separation edge. Results are presented in figure 2. The time-mean velocity Q attains a sharp maximum at the edge of the boundary layer at separation, which could be a candidate for the reference position. At this position, however, q' is of the order of 10% of the main-flow velocity at $Re = 2.76 \times 10^5$, so it was suspected that the sinusoidal velocity disturbance due to the forcing might be overcome by this turbulence. Thus the position (outside the boundary layer) where Q is 90% of its maximum value was chosen as the reference position; at this position q' is (0.006–0.009) U_∞ in the present range of Reynolds number. The reference position is only slightly dependent on Reynolds number, being located approximately at $(x/d, r/d) = (-0.008, 0.5)$. It may be noted that the same distributions of Q and q' were not measured in the forced flow. Thus it is not clear whether the reference position is still a well-behaved position in the forced flow.

At the reference position, the velocity fluctuation generated by the forcing was sinusoidal to the extent that its power spectrum had a sharp peak at the forcing

https://doi.org/10.1017/S0022112097005521 Published online by Cambridge University Press

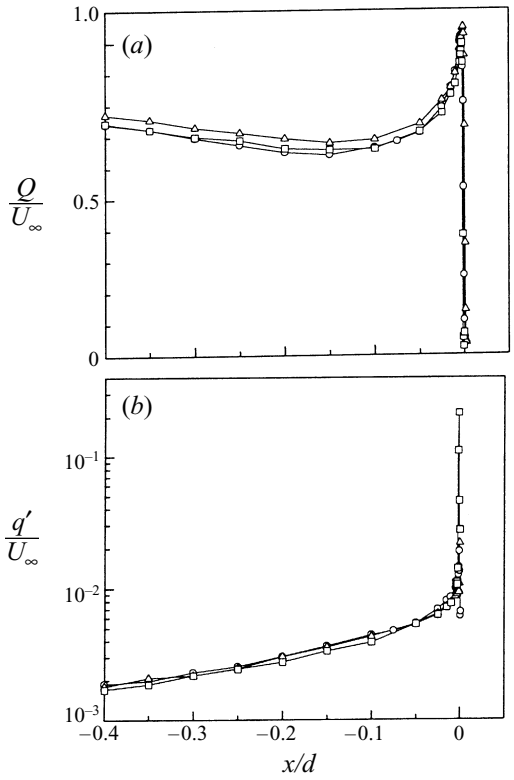


FIGURE 2. Distributions of (*a*) time-mean velocity Q and (*b*) r.m.s. fluctuating velocity q' of unforced flow near the separation edge. ○, $Re = 0.69 \times 10^5$; △, 1.38×10^5; □, 2.76×10^5.

frequency with insignificant peaks at higher- and sub-harmonics. Thus the velocity fluctuation due to the forcing q is written, for the single-frequency forcing, as

$$q = q_1 \sin(2\pi f_1 t),$$

and, for the double-frequency forcing, as

$$q = q_1 \sin(2\pi f_1 t) + q_2 \sin(2\pi f_2 t + \phi),$$

where q_1 and q_2 are forcing amplitudes, f_1 and f_2 ($> f_1$) are forcing frequencies, ϕ is phase difference, and t is time. In the double-frequency forcing, q_2 was chosen to be equal to q_1 for simplicity. The forcing level is represented by the r.m.s. amplitude $q_1' = q_1/\sqrt{2}$ for both the single- and double-frequency forcing. Samples of the velocity fluctuation q and its amplitude spectrum are shown in figure 3 for the single-frequency and double-frequency forcing.

2.3. *Definition of reattachment position*

In this study, the reattachment position is defined as the position where the reverse-flow intermittency measured near the surface I_r attains the value of 0.5. The split-film probe was used to measure the instantaneous longitudinal velocity along a longitudinal line at 1 mm or $0.005d$ above the cylinder surface, I_r being calculated from the time history of this velocity. The present definition of reattachment position is different from the conventional one that reattachment occurs at the position where the time-mean surface shear stress is zero (Ruderich & Fernholz 1986). At the reattachment position, however, both the time-mean longitudinal velocity U and its normal gradient

https://doi.org/10.1017/S0022112097005521 Published online by Cambridge University Press

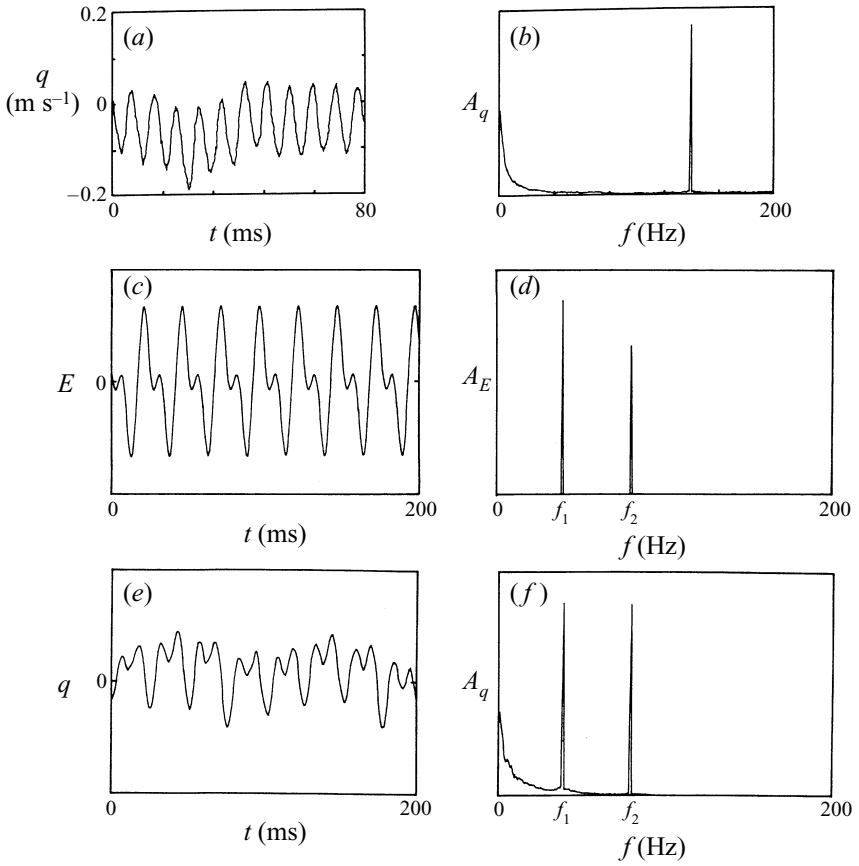


FIGURE 3. Samples of the time history of the fluctuating velocity q at the reference position and its amplitude spectrum for forced flow. (*a*) q and (*b*) its spectrum A_q for single-frequency forcing with $f_1 = 140$ Hz; (*c*) input voltage E to woofer, (*d*) its spectrum A_E; (*e*) q, and (*f*) its spectrum A_q for double-frequency forcing with $f_1 = 40$ Hz, $f_2 = 80$ Hz. The vertical axis in (*b*)–(*f*) is arbitrary linear.

$\partial U/\partial r$ are zero at the surface, so that U near the surface is approximately equal to zero (see, for example, figure 15 of Ruderich & Fernholz 1986). Thus the position of $I_r = 0.5$ near the surface is expected to be a good approximation to the true reattachment position. Indeed this definition of the reattachment position has been shown to be in good agreement with a flow-visualization experiment (Kiya & Sasaki 1983).

3. Results for single-frequency forcing

3.1. *Reattachment length as a function of forcing amplitude and frequency*

The reattachment length x_R is shown in figure 4 as a function of the forcing amplitude and frequency. In figure 4(*a*), the forcing amplitude is in the range $q_1'/U_\infty = 0.005$–0.10, while it is in the higher range $q_1'/U_\infty = 0.12$–0.20 in figure 4(*b*), where the result for $q_1'/U_\infty = 0.10$ is also included for comparison. The reattachment length is normalized by that of the unforced flow x_{R0}, which was $(1.60 \pm 0.06)\,d$ in the present range of Reynolds number; the forcing frequency is normalized in the form $f_1 d/U_\infty$.

In the lower range of the forcing amplitude (figure 4*a*), the reattachment length

https://doi.org/10.1017/S0022112097005521 Published online by Cambridge University Press

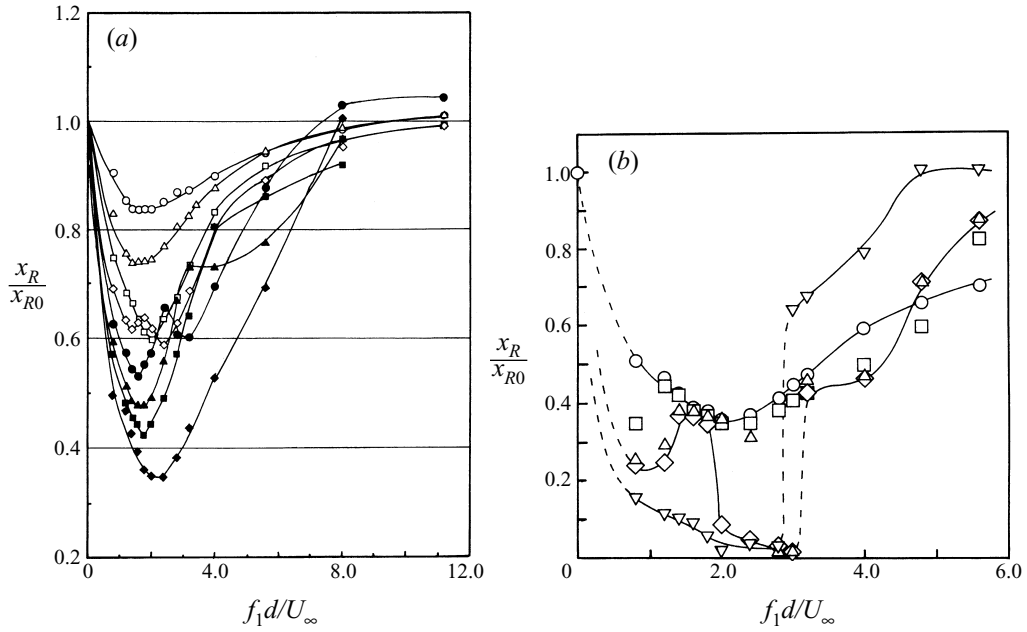


FIGURE 4. Reattachment length x_R as function of the forcing frequency f_1 and amplitude q_1' at $Re = 0.69 \times 10^5$. (*a*) ○, $q_1'/U_\infty = 0.005$; △, 0.01; □, 0.02; ◇, 0.03; ●, 0.04; ▲, 0.05; ■, 0.06; ◆, 0.10; (*b*) ○, $q_1'/U_\infty = 0.10$; □, 0.12; ◇, 0.14; △, 0.15; ▽, 0.20.

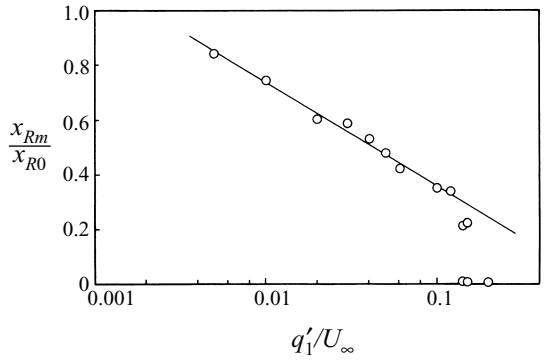


FIGURE 5. Minimum reattachment length x_{Rm} as function of the forcing amplitude at $Re = 0.69 \times 10^5$. The solid straight line is a least-squares fit in the range $q_1'/U_\infty \leqslant 0.12$.

attains a minimum at a particular forcing frequency which seems to depend slightly on the forcing amplitude. This frequency will be referred to as the most effective frequency *F*. Sigurdson (1995) has suggested that the drag acting on the front face of the cylinder attains a minimum value at the same frequency *F*.

In the higher range of the forcing amplitude (figure 4*b*), the reattachment length responds to the forcing frequency in a more complicated manner. It is noteworthy that, for forcing amplitudes greater than $q_1'/U_\infty = 0.14$, x_R becomes almost zero in a range of the forcing frequency (figure 4*b*). Thus, in this case, one cannot define a single frequency as the most effective frequency *F*. Furthermore, it is interesting to note that a dip of x_R appears approximately at the frequency $f_1 d/U_\infty \approx 1.0$.

The minimum reattachment length x_{Rm} is plotted in figure 5 against the forcing amplitude. For the amplitudes $q_1'/U_\infty = 0.12$–0.15, the value of x_R at the above-

https://doi.org/10.1017/S0022112097005521 Published online by Cambridge University Press

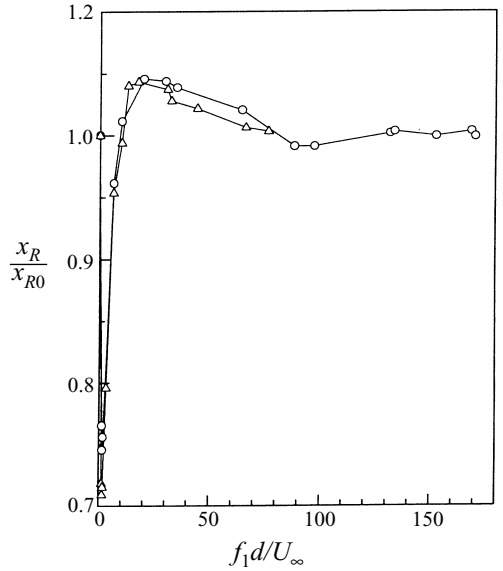


FIGURE 6. Reattachment length as function of forcing frequency. $q_1'/U_\infty = 0.01$. ○, $Re = 0.69 \times 10^5$; △, $Re = 1.38 \times 10^5$.

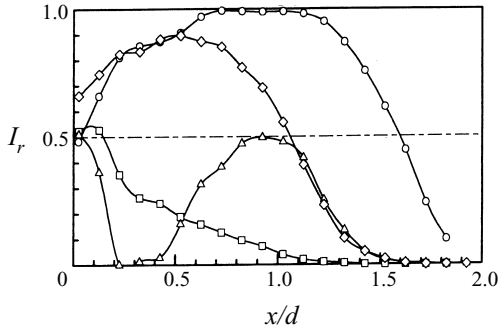


FIGURE 7. Distributions of reverse-flow intermittency I_r. $q_1'/U_\infty = 0.20$. $Re = 0.69 \times 10^5$. ○, Unforced flow; □, $f_1 d/U_\infty = 1.6$; △, 2.8; ◇, 3.2.

mentioned dip is also included. The minimum reattachment length can be represented by the empirical formula $x_{Rm}/x_{R0} = -0.371 \ln (q_1'/U_\infty) - 0.007$ for amplitudes $q_1'/U_\infty \leqslant 0.12$. Thus the maximum reduction in the reattachment length can be written in the normalized form $(x_{R0} - x_{Rm})/x_{R0} = 1.007 + 0.371 \ln (q_1'/U_\infty)$. This logarithmic dependence is different from the linear dependence of the maximum reduction in the drag of the front face (figure 13 of Sigurdson 1995).

The forcing frequency is extended up to $f_1 d/U_\infty = 170$ in figure 6. The reattachment length is independent of the forcing frequency in the range $f_1 d/U_\infty > 80$. This value of 80 is approximately twice the frequency of the initial Kelvin–Helmholtz instability f_{KH} of the separated shear layer, which was approximately $f_{KH} d/U_\infty = 31$ and 44 at $Re = 0.69 \times 10^5$ and 1.38×10^5, respectively. The independence is because there is no instability to amplify the forcing for a frequency greater than f_{KH}, as discussed by Sigurdson (1995). It is worth noting that x_R attains a maximum greater by 4% than that of the unforced flow at f_1 of the order of $f_{KH}/2$. This feature remains to be explained.

https://doi.org/10.1017/S0022112097005521 Published online by Cambridge University Press

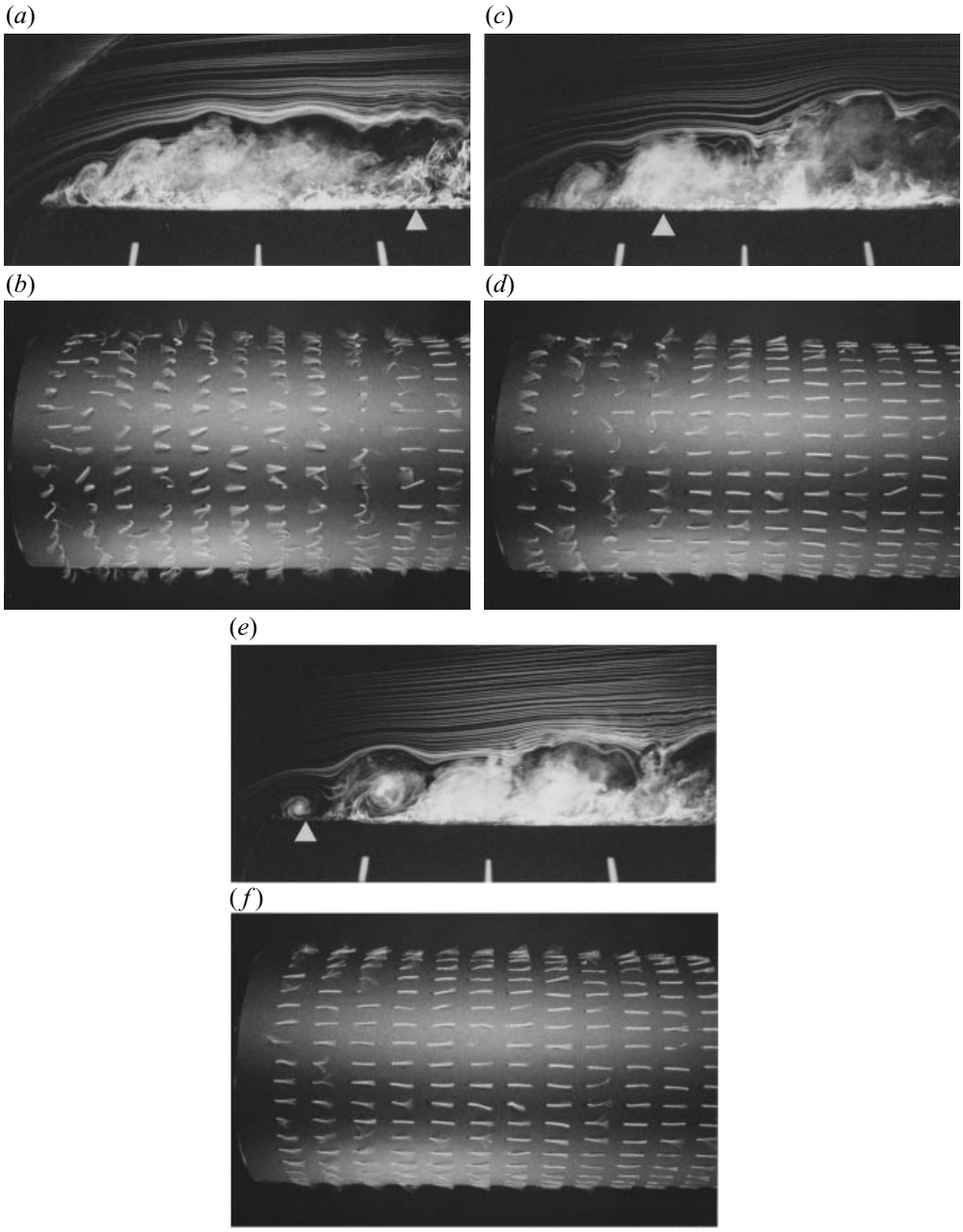


FIGURE 8. Snapshots of flow visualized (a, c, e) by smoke ($Re = 1.4 \times 10^4$), and (b, d, f) by tufts on the surface ($Re = 0.69 \times 10^5$). (a, b) Unforced flow; (c, d) flow forced by $(q_1'/U_\infty, f_1 d/U_\infty) = (0.10, 2.0)$; ($e$, f) (0.20, 1.6). The white triangle indicates the reattachment position; white vertical marks indicate positions $x/d = 0.5$, 1.0 and 1.5.

3.2. *Flow field*

Results will be presented mainly for the flow forced with the amplitude $q_1'/U_\infty = 0.20$ in comparison with the unforced flow.

Figure 7 shows the reverse-flow intermittency I_r plotted against x. At the fre-

https://doi.org/10.1017/S0022112097005521 Published online by Cambridge University Press

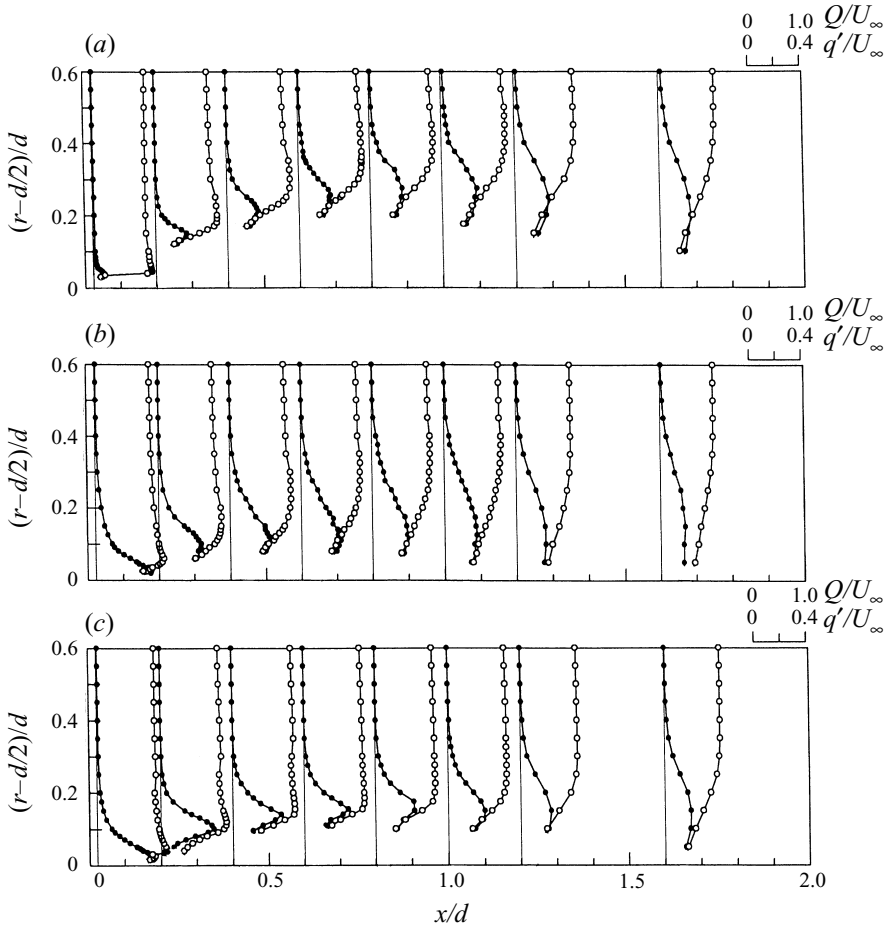


FIGURE 9. Distributions of time-mean and r.m.s. velocities in (*a*) unforced flow, (*b*) flow forced by $(q_1'/U_\infty, f_1 d/U_\infty) = (0.20, 1.6)$, and (*c*) (0.20, 2.8). $Re = 0.69 \times 10^5$. ○, Q; ●, q'. Measurements were made by single I-type hot-wire probe, so that velocities are shown only in regions where reverse flow is insignificant. Note that reverse-flow intermittency for these flows is shown in figure 7.

quency $f_1 d/U_\infty = 1.6$, I_r is only slightly greater than 0.5 in a narrow region immediately behind the leading edge $x = 0$, decreasing monotonically downstream of this region; this demonstrates the existence of a very weak reverse flow only in this narrow region. At higher values of f_1 a hump appears in the distribution of I_r, as in the case of $f_1 d/U_\infty = 2.8$. The height of the hump increases with increasing f_1, so that I_r attains a distribution like that for $f_1 d/U_\infty = 3.2$. This change in the distributions of I_r corresponds to the sudden change in x_R at $f_1 d/U_\infty \approx 3.0$, see figure 4(*b*). In the intermediate range $2.8 < f_1 d/U_\infty < 3.2$, there exists a recirculating region detached from the leading edge.

Figure 8 shows the flow visualization. The formation of large vortices by the forcing and the reduction of the reverse-flow region are clearly demonstrated. The very short separation bubble in figure 8(*e*) is accompanied by the formation of a compact and strong vortex near the leading edge. This vortex interacts with the surface immediately as it rolls up, travelling downstream without amalgamation. Thus the distance between two consecutive vortices in figure 8(*e*) is equal to the wavelength of the disturbance produced by the forcing.

https://doi.org/10.1017/S0022112097005521 Published online by Cambridge University Press

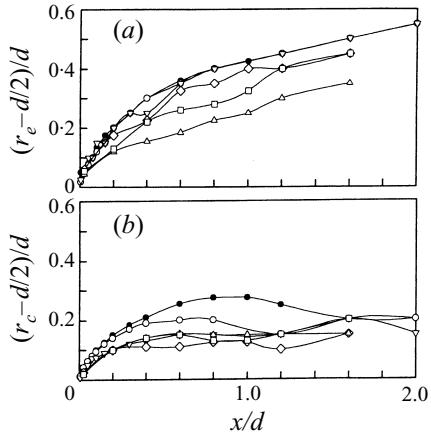


FIGURE 10. Distributions of (*a*) the edge of the shear layer r_e, and (*b*) the position of maximum r.m.s. velocity r_c. $Re = 0.69 \times 10^5$. ●, Unforced flow; ○, flow forced by $(q_1'/U_\infty, f_1 d/U_\infty) = (0.10, 1.6)$; ◇, (0.20, 1.6); △, (0.20, 2.8); □, (0.20, 3.2).

Distributions of the time-mean and r.m.s. velocities, Q and q', are shown in figure 9. Note that these velocities were measured by the I-type hot-wire probe, so that they are affected by the rectifying effects of the probe in a region where the flow is intermittently reversed. Thus the velocities are shown only in regions where the reverse flow is expected to be insignificant. It may be noted that I_r is less than 0.1 at the position of maximum r.m.s. velocity, r_c, in the separation bubble of a blunt plate (Kiya & Sasaki 1983). This suggests that Q and q' in the region $r \geqslant r_c$ are fairly reliable because the separation bubble of the blunt circular cylinder has basically similar properties to that of the blunt plate (Kiya 1989). It may be noted that no time-mean reverse flow exists in the forced flows (figure 9*b*, *c*) except for the narrow region behind the separation edge.

The maximum r.m.s. velocity is much higher in the forced flow than in the unforced flow, amounting to approximately $0.40U_\infty$ near the edge (figure 9*b*, *c*). This maximum value is the same as that which can be realized in the separated shear layer forced by an external sound wave (Nishioka *et al.* 1990). It is surprising that, at $f_1 d/U_\infty = 2.8$, the maximum of q' appears at the edge of the shear layer in the region $x/d \leqslant 0.8$, while in the other cases (figure 9*a*, *b*) the maximum appears at the position where $\partial Q/\partial r$ attains a maximum, as would be expected in the separated shear layers (Kiya & Sasaki 1983; Ruderich & Fernholz 1986). This might be associated with the forcing-induced flapping motion of the shear layer whose velocity fluctuation is superposed on that generated by the forcing-induced vortices. The contribution of the flapping motion to the overall velocity fluctuation possibly depends on f_1 even if q_1' is fixed. Moreover, a long tail in the profile of q' near the edge (figure 9*b*, *c*) demonstrates the extent to which the disturbance produced by the forcing penetrates into the main flow.

Figure 10 shows the position of the edge of the shear layer r_e and the position of the maximum r.m.s. velocity r_c. With forcing at $q_1'/U_\infty = 0.20$, the distance between r_c and the surface is reduced by approximately 50 % in the region $x/d < 1.2$ as compared to the case of the unforced flow. The edge approaches nearest to the surface at the forcing frequency $f_1 d/U_\infty = 2.8$.

The cross-correlation of q at two points separated in the circumferential direction, R, is presented in figure 11. Here R is the cross-correlation at zero time delay, and Δ is the angle between the two points. R was measured near the edge of the shear layer at the middle and the end of the separation bubble. However, in the cases of $(q_1'/U_\infty,$

https://doi.org/10.1017/S0022112097005521 Published online by Cambridge University Press

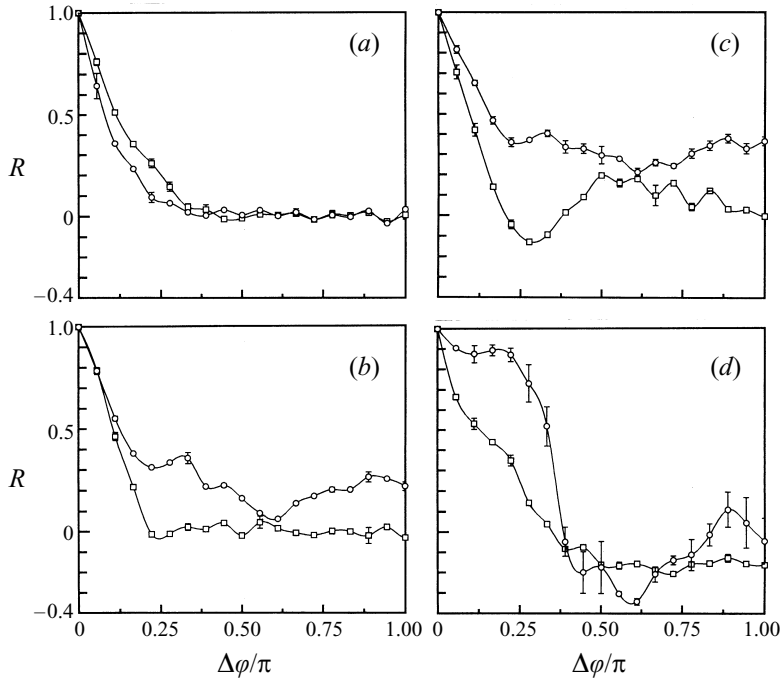


FIGURE 11. Cross-correlation of velocity fluctuations q at two points at the edge of the shear layer, R, for (a) unforced flow, (b) flow forced by $(q_1'/U_\infty, f_1 d/U_\infty) = (0.10, 2.0)$, ($c$) (0.20, 1.6), and ($d$) (0.20, 2.8). $Re = 0.69 \times 10^5$. ○, $x = x_R/2$ in (a, b) and $x = d/2$ in (c, d); □, $x = x_R$ in (a, b) and $x = d$ in (c, d).

$f_1 d/U_\infty) = (0.20, 1.6)$ and $(0.20, 2.8)$, x_R is so short that R is obtained at $x = d/2$ and d. In the unforced flow, R is seen to be zero for angles $\Delta > \pi/3$. In the forced flows, on the other hand, a long tail of positive R appears at $x = x_R/2$ and $x = d/2$, extending up to $\Delta = \pi$ (figure 11b, c); R decays much faster at the downstream positions $x = x_R$ and $x = d$. This indicates the enhanced axisymmetry of the rolling-up vortices in the forced flows and the subsequent breakdown of the vortices. High values of R in figure 11(d) in the range of $\Delta < \pi/3$ suggest the formation of the most coherent vortices in this case among the forced flows.

A measure of the circumferential coherence is given by the integral scale Φ that is the integral of R with respect to Δ from 0 to Δ_0, which is the value of Δ where R first becomes zero. If R is positive up to $\Delta = \pi$, Δ_0 is taken as π. The integral scale is shown in figure 12 plotted against x. In the unforced flow, Φ is fairly constant, being of the order of 0.15π. However, in the forced flows, Φ attains a much higher value of approximately $(0.3\text{–}0.4)\,\pi$ at the positions $x = x_R/2$ and $x = d/2$. The sudden drop of Φ at the downstream positions $x = x_R$ and $x = d$ reflects the breakdown of the rolled-up vortices. After the breakdown, Φ becomes approximately the same for forced and unforced flows. This value of Φ is equivalent to $0.17x_{R0}$, which happens to be approximately equal to the distance between r_c and the surface of the unforced flow (which is a measure of the height of the separation bubble), namely $0.16x_{R0}$ ($= 0.26D$, see figure 10b).

https://doi.org/10.1017/S0022112097005521 Published online by Cambridge University Press

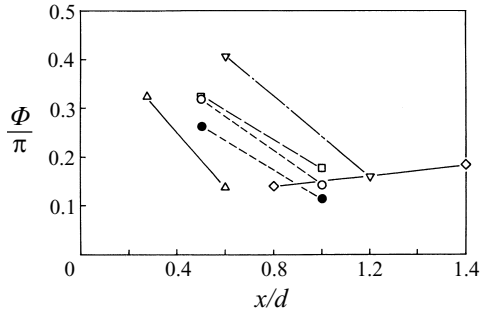


FIGURE 12. Distribution of the integral scale of the cross-correlation Φ. $Re = 0.69 \times 10^5$. $\diamond$, Unforced flow; $\triangledown$, flow forced by $(q_1'/U_\infty, f_1 d/U_\infty) = 0.01, 1.6)$; $\triangle$, (0.10, 2.0); $\bigcirc$, (0.20, 1.6); $\square$, (0.20, 2.8); $\bullet$, (0.20, 3.2).

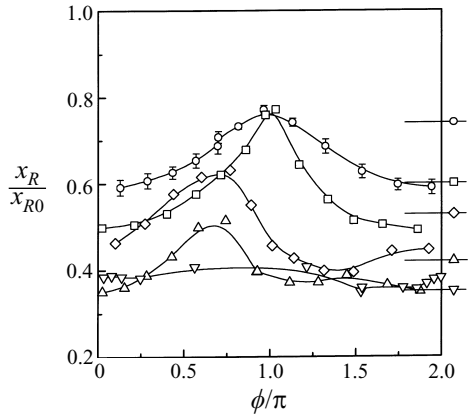


FIGURE 13. Reattachment length as function of forcing amplitude and phase difference for double-frequency forcing. $f_1 = F$, $f_2 = 2F$. $Re = 0.69 \times 10^5$. $\bigcirc$, $q_1'/U_\infty = 0.01$; $\square$, 0.02; $\diamond$, 0.04; $\triangle$, 0.06; $\triangledown$, 0.10. Horizontal line segments on the right imply the reattachment length for the single-frequency forcing with $f_1 = F$.

4. Results for double-frequency forcing

In the double-frequency forcing, the following combinations of frequencies are studied: $(f_1, f_2) = (F, 2F)$, $(F, 3F)$, $(F, 4F)$, $(F/2, 2F)$, $(F, F+F/8)$, and $(F-F/8, F)$, where F is the most effective frequency described in §3. It may be noted that, for the last two combinations, the phase difference ϕ has no meaning.

Figure 13 shows the relation between x_R and ϕ for the combination $(F, 2F)$. At low forcing amplitudes $q_1'/U_\infty = 0.01$ and 0.02, x_R attains a maximum at $\phi \approx \pi$, and a broad minimum at $\phi \approx 0$. However, at the high amplitude $q_1'/U_\infty = 0.10$, x_R is independent of ϕ, being approximately the same as that for the single-frequency forcing with $f_1 = F$. At intermediate amplitudes $q_1'/U_\infty = 0.04$ and 0.06, a maximum of x_R appears at the smaller phase difference $\phi \approx 2\pi/3$. These properties will be discussed in §5.2.

Results for the combination $(F, 3F)$ are presented in figure 14. The reattachment length is seen to depend only weakly on ϕ. Moreover, x_R is not much different from the minimum reattachment length for the single-frequency forcing.

Results for the other combinations of frequencies are summarized in figure 15 for the forcing amplitude $q_1'/U_\infty = 0.01$. For all these combinations, x_R appears to be independent of ϕ. For the non-resonant combinations $(F-F/8, F)$ and $(F, F+F/8)$, x_R

https://doi.org/10.1017/S0022112097005521 Published online by Cambridge University Press

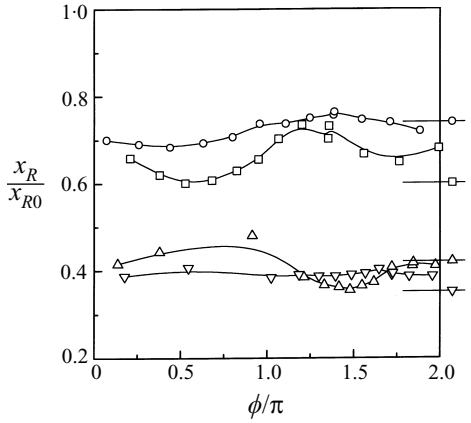


FIGURE 14. Reattachment length as function of q_1'/U_∞ and ϕ for double-frequency forcing. $f_1 = F, f_2 = 3F$. $Re = 0.69 \times 10^5$. ○, $q_1'/U_\infty = 0.01$; □, 0.02; △, 0.06; ▽, 0.10.

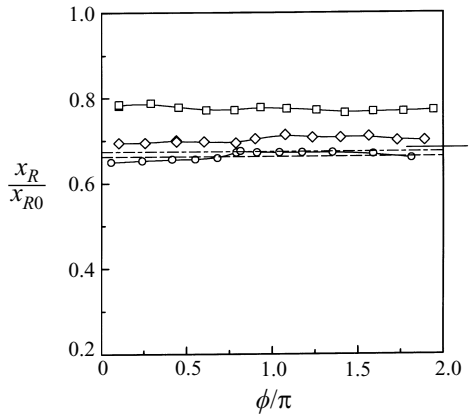


FIGURE 15. Reattachment length as function of ϕ for double-frequency forcing. $q_1'/U_\infty = 0.01$. $Re = 0.69 \times 10^5$. ○, $(f_1, f_2) = (F, F/2)$; □, $(F, 4F)$; ◇, $(F/2, 2F)$; ———, $(F-F/8, F)$; – – –, $(F, F+F/8)$.

is approximately the same as the minimum reattachment length for the single-frequency forcing with the equivalent r.m.s. amplitude $q_1'/U_\infty = \sqrt{2} \times 0.01$.

5. Discussion

5.1. *Interpretation of the most effective frequency*

As has been discussed by Sigurdson (1995), there are two instabilities in the separation bubble: one is the initial Kelvin–Helmholtz instability, and the other is the shedding-type instability. Owing to the shedding-type instability, large vortices are shed from the reattachment region with the frequency f_v. He presumes that the shedding-type instability is the same as that which causes the periodic vortex shedding from two-dimensional bluff bodies such as a circular cylinder. The frequency of the shedding-type instability is a function of the velocity at the separation edge U_s and the height of the separation bubble obtained by Roshko's (1954) hodograph method h, having the universal value of $f_v h/U_s = 0.08$ (Roshko 1955). At high Reynolds numbers, f_v is much lower than and irrelevant compared to the initial Kelvin–Helmholtz frequencies f_{KH}.

https://doi.org/10.1017/S0022112097005521 Published online by Cambridge University Press

Sigurdson (1995) suggests that the maximum reduction in the drag or in the reattachment length occurs at the forcing frequency F given by $Fh/U_s = 0.08$. However, the most effective frequency in his experiment is 2 to 5 times the expected value of 0.08 for the most amplified shedding frequency. He argues that the minimum drag occurs when the initial shear layer is used to amplify the forcing, creating structures that amalgamate to form a final structure with $f_v h/U_s = 0.08$. He also suggests that the most effective frequency must be greater than the first harmonic of f_v, since each shed structure often consists of a pairing of the final two shear-layer structures before reattachment.

To supplement Sigurdson's (1995) discussion, a flow model is presented here to explain the most effective frequency under two main hypotheses. The first hypothesis is that the separation bubble is a self-excited flow maintained by a feedback loop, this being the case for both the forced and unforced flows. When a large vortex impinges on the surface in the reattachment region, a pressure fluctuation is generated, propagating upstream with the speed of sound a. This pressure fluctuation is accepted by the flow at the sharp separation edge, modifying the rolling-up of the shear layer. This is the receptivity issue (Nishioka & Morkovin 1986). One may suspect that, if the forcing amplitude is sufficiently high, the amalgamation of vortices produced by the forcing would hardly be influenced by a disturbance accepted at the separation edge. However, it is possible that the role of the forcing is just to produce the rolling-up vortices, the subsequent amalgamation of the vortices being governed by the accepted disturbance.

The above-mentioned feedback system can be formulated as follows. The pressure fluctuation propagates from the reattachment position to the separation edge in the time x_R/a, generating a vorticity disturbance at the edge. This disturbance is convected downstream with an average velocity U_c to arrive at the reattachment position at the time x_R/U_c. Thus the time $x_R/U_c + x_R/a$ should be equal to the integral multiple of the period of the self-excited flow. If the fundamental frequency of this self-excited system is taken as the vortex-shedding frequency f_v, one obtains the feedback equation

$$x_R/U_c + x_R/a = N/f_v, \tag{1}$$

where N is an integer. With $U_c \ll a$ and $N = 1$ equation (1) reduces to

$$f_v x_R/U_\infty = U_c/U_\infty. \tag{2}$$

The self-excited flow seems to be consistent with the concept of the impinging-shear-layer instability suggested by Nakamura & Nakashima (1986).

In the unforced flow, the average convection velocity is $U_c/U_\infty \approx 0.5$ (Kiya & Nozawa 1987), so that $f_v x_{R0}/U_\infty \approx 0.5$. This value is observed in a wide range of unforced separation bubbles (Cherry, Hillier & Latour 1984; Kiya 1989), suggesting that the feedback mechanism is universal.

The forced flow can also be interpreted as the self-excited flow maintained by the feedback loop, as demonstrated in figure 16 which is the vortex-shedding frequency $f_v x_R/U_\infty$ plotted against the forcing amplitude. The fairly large uncertainty of the data is due to the uncertainty in determining f_v. Although $f_v x_R/U_\infty$ seems to decrease slightly with increasing q_1'/U_∞, its average value is 0.46. The decrease in $f_v x_R/U_\infty$ is conjectured to be due to the effect of those image vortices inside the cylinder whose circulation is enhanced by the forcing, reducing the convection velocity.

The second hypothesis is that the minimum reattachment length is realized when the vortex shed from the reattachment region has just been created by the nth amalgamation of the rolled-up vortices right at the reattachment position, which is the

https://doi.org/10.1017/S0022112097005521 Published online by Cambridge University Press

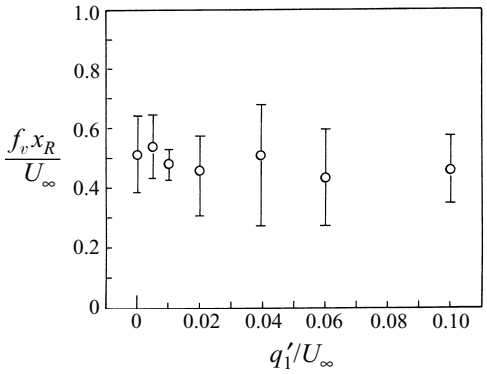


FIGURE 16. Normalized vortex-shedding frequency $f_v x_R/U_\infty$ as function of forcing amplitude q_1'/U_∞. $Re = 0.69 \times 10^5$.

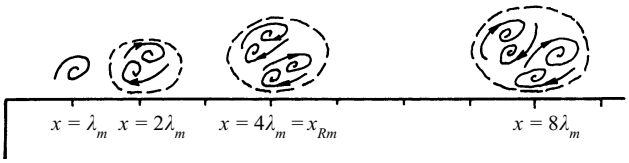


FIGURE 17. Illustration of the relation between positions of $x = x_{Rm}$ and vortex amalgamation. In this example, reattachment occurs at $x = 4\lambda_m$.

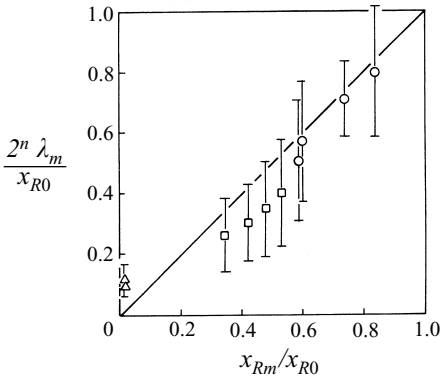


FIGURE 18. Comparison of experimental values of minimum reattachment length with those predicted by the flow model. Solid line shows perfect correlation. ○, $n = 2$; □, $n = 1$; △, $n = 0$.

longitudinal position of centre of the shed vortex. This is illustrated in figure 17 for the case of $n = 2$. The value of n is a function of the forcing amplitude but cannot be determined within the framework of this model. If two vortices are involved in each amalgamation, the minimum reattachment length x_{Rm} is given by

$$x_{Rm} = 2^n \lambda_m, \tag{3}$$

where λ_m $(= U_c/F)$ is the wavelength of the disturbance produced by forcing with the most effective frequency. This equation can be written in the form

$$x_{Rm} F/U_\infty = 2^n U_c/U_\infty. \tag{4}$$

Equation (3) is not inconsistent with the experiment, as shown in figure 18, in which the reattachment length of the flow model is calculated by putting $n = 2$ for

https://doi.org/10.1017/S0022112097005521 Published online by Cambridge University Press

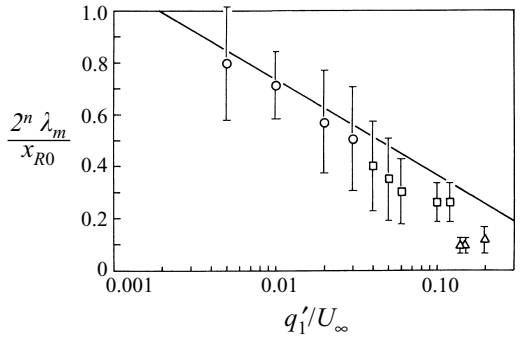


FIGURE 19. Minimum reattachment length predicted by the flow model as function of forcing amplitude. The solid line is the same as in figure 5. Symbols as in figure 18.

$q_1'/U_\infty = 0.005$–0.03, $n = 1$ for $q_1'/U_\infty = 0.04$–0.12, and $n = 0$ for $q_1'/U_\infty = 0.14$–0.20 to have the best fit between the model and experiment. Here it may be worth noting that two minima of x_R appear for $q_1'/U_\infty = 0.03$–0.04 (figure 4*a*), which demarcate $n = 1$ and $n = 2$.

Equations (2) and (4) yield

$$F/f_v = 2^n, \tag{5}$$

if x_R in equation (3) is put equal to x_{Rm}. Equation (5) implies that the most effective frequency scales with the vortex-shedding as discussed by Sigurdson & Roshko (1988) and Sigurdson (1995).

The minimum reattachment length obtained from this flow model is shown as a function of q_1'/U_∞ in figure 19. The uncertainty in the data is again due to that in determining f_v. The flow model is seen to yield the minimum reattachment length in fair agreement with the experimental results.

The flow model discussed above is still a preliminary one, including a few hypotheses. However, we feel that this can be a first step in constructing a more reasonable theory on the forced separation bubbles.

5.2. *The role of phase difference in double-frequency forcing*

The effects of the phase difference on the reattachment length can be understood at least qualitatively in terms of the response of a two-dimensional mixing layer to the double-frequency forcing. This is not unreasonable because the height of the separation bubble is less than $0.26D$ (figure 10*b*) and the circumferential integral scale Φ is less than 0.4π (figure 12).

First, the case of the combination $(F, 2F)$ will be considered (figure 13). Riley & Metcalfe (1980) have conducted a direct numerical simulation of the vortex-amalgamation interaction in a time-evolving two-dimensional mixing layer forced by a combination of the fundamental and the first subharmonic, whose amplitudes are in the regime of linear instability. The fundamental frequency is the frequency at which the linear instability mode has the maximum growth rate (Ho & Huang 1982). Riley & Metcalfe (1980) demonstrate that, when the two components are in antiphase ($\phi = \pi$), the vortex amalgamation is suppressed and replaced by a shredding interaction, in which vortices generated by the fundamental are alternately shredded in the straining field of the subharmonic. On the other hand, the vortex amalgamation is most enhanced at $\phi = 0$. This is the subharmonic resonance found by Kelly (1967). Thus, if the fundamental and the first subharmonic are interpreted as the $2F$- and F-components in the forced shear layer of the separation bubble, the vortices produced

https://doi.org/10.1017/S0022112097005521 Published online by Cambridge University Press

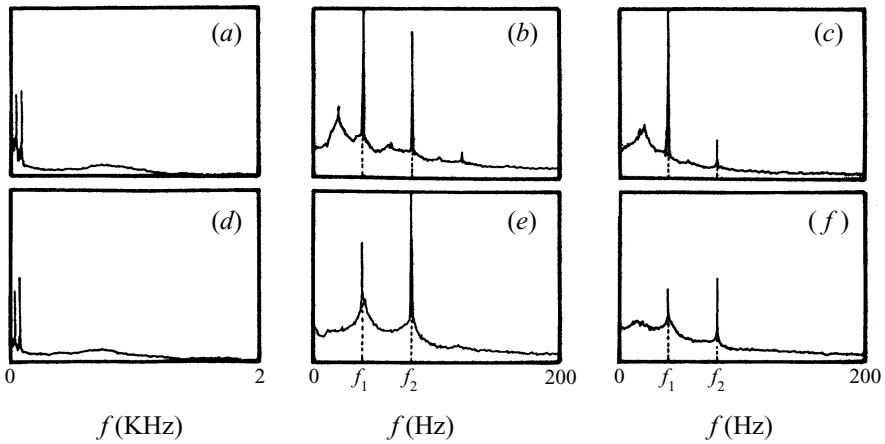


FIGURE 20. Evolution of the amplitude spectrum of q at the edge of the shear layer for double-frequency forcing. $f_1 = F$, $f_2 = 2F$, $q_1'/U_\infty = 0.01$, $Re = 0.69 \times 10^5$. (a, b, c) $\phi = 0$; (d, e, f) $\phi = \pi$. (a, d) $x/d = 0.005$; (b, e) $x/d = 0.30$; (c, f) $x/d = 0.60$. The vertical scale is arbitrary linear.

by the $2F$-component are expected to be alternately shredded by the straining field of the F-component at $\phi = \pi$, while their amalgamation is most enhanced at $\phi = 0$. This is demonstrated by the evolution of the amplitude spectrum of the velocity fluctuation q (see figure 20). The larger the vortices, the larger is the entrainment, so that the maximum and the minimum of x_R are expected to appear at $\phi = \pi$ and 0, respectively. This is the case for the low amplitude $q_1'/U_\infty = 0.01$–0.02, as seen in figure 13.

The fact that x_R becomes independent of ϕ at the high amplitude $q_1'/U_\infty = 0.10$ (figure 13) seems to correspond to the finding of Raman & Rice (1989) and Paschereit, Wygnanski & Fiedler (1995) in their studies of the double-frequency forcing of the spatially evolving axisymmetric mixing layer of a round jet. In these studies the momentum thickness is much lower than the radius of the nozzle, so that the mixing layer can be interpreted as a plane mixing layer. Their studies show that an increase in the forcing amplitude reduces the effect of the initial phase difference on the amplification of the subharmonic. This suggests that, in the forced shear layer, the effect of the F-component on the amalgamation of the vortices generated by the $2F$-component is independent of the phase difference at sufficiently high forcing amplitudes. However, the shift of the maximum of x_R towards the low range of ϕ at the intermediate amplitudes $q_1'/U_\infty = 0.04$–0.06 remains to be explained.

The insignificant dependence of x_R on the phase difference for the combinations $(F, 3F)$ and $(F, 4F)$ (figures 14 and 15) can be understood in terms of Inoue's (1992) numerical simulation of a spatially evolving two-dimensional mixing layer forced by a double-frequency disturbance. He shows that the momentum thickness of the mixing layer for $(F, 3F)$ and $(F, 4F)$ is independent of ϕ over a normalized longitudinal distance from the edge of the splitter plate, say x^*, of 75 and 110, respectively, while for the combination $(F, 2F)$ the effect of ϕ on the momentum thickness appears at the much shorter distance $x^* = 25$ (see figure 13 of Inoue 1992). If the reattachment of the separated shear layer were to occur earlier than $x^* = 75$ for $(F, 3F)$, x_R would be expected to be independent of ϕ; if the reattachment were to occur downstream of $x^* = 75$, x_R would be somewhat influenced by ϕ. This may explain the result of figure 14. The same argument can be applied to understand the result of figure 15 for $(F, 4F)$.

https://doi.org/10.1017/S0022112097005521 Published online by Cambridge University Press

6. Conclusion

The response of the leading-edge separation bubble of a blunt circular cylinder to single- and double-frequency forcing has been studied experimentally. The response is mainly described in terms of the relation between the reattachment length and the forcing frequency and amplitude. In his recent paper on the same flow configuration, Sigurdson (1995) concentrates on the reduction in the drag force acting on the front face of a blunt circular cylinder by the single-frequency forcing. In the present paper, the r.m.s. forcing amplitude q_1' is varied from 0.5 to 20% of the main-flow velocity, while the forcing frequency f_1 is extended up to more than four times the frequency of the initial Kelvin–Helmholtz instability. In the double-frequency forcing, two sinusoidal components have the same amplitude. The wide range of the forcing frequency and amplitude has revealed several striking aspects of the forced separation bubble.

The forced and unforced flows can be interpreted as self-excited flows maintained by a feedback loop. This interpretation yields a simple expression for the frequency of shedding of rolled-up vortices from the separation bubble f_v as a function of x_R and U_∞, see equation (2). This expression is compatible with equation (9) of Sigurdson (1995), explaining why a fairly universal value of $f_v x_R/U_\infty \approx 0.5$ is found in a wide range of separation bubbles.

The reattachment length attains a minimum at a particular forcing frequency F which is in the range 1.6–2.2 in the normalized form Fd/U_∞ if q_1' is less than $0.12U_\infty$. This most effective frequency F scales with the frequency of shedding of rolled-up vortices from the separation bubble f_v in the form $2^n f_v$, where n is an integer depending on q_1'. Sigurdson (1995) seems to suggest the same relation between F and f_v, but not explicitly giving the factor 2^n.

The minimum reattachment length x_{Rm} is represented by a logarithmic function of q_1'/U_∞. This is not the case for the maximum drag reduction, which is a linear function of q_1'/U_∞ (Sigurdson 1995).

The reverse-flow region is almost eliminated in a range of the forcing frequency if $q_1'/U_\infty \geqslant 0.14$. In this case, a compact vortex is formed right at the separation edge, as demonstrated in figure 8(*e*) (also see figure 6*b* of Sigurdson 1995; figure 11 of Nishioka *et al.* 1990); at the same time, the distance between the edge of the shear layer and the surface becomes approximately half of that for the unforced flow.

The rolled-up vortices generated by the forcing are highly coherent in the circumferential direction in the middle of the separation bubble, the integral scale Φ being $(0.3–0.4)\pi$. However, the high coherence is quickly destroyed at the end of the bubble, Φ reducing to approximately half of the above value. This reduced value happens to be the same as that for the unforced flow.

The double-frequency forcing is most effective for superposition of the F-component on its higher harmonic ($2F$) in the sense that x_R is most strongly dependent on the phase difference ϕ. A minimum and a maximum of x_R appear at $\phi = 0$ and π, respectively. However, the combination of the F-component and the higher harmonics $3F$ or $4F$ yields an insignificant dependence of x_R on ϕ. It seems that these features can be explained, at least qualitatively, in terms of the response of a two-dimensional mixing layer to double-frequency forcing.

This study was supported by the Grant-in-Aid for Scientific Studies from the Ministry of Education, Science and Culture (Category B, Project Number 05452148). Professor Fazle Hussain, University of Houston, gave valuable advice at the initial

https://doi.org/10.1017/S0022112097005521 Published online by Cambridge University Press

stage of this study; this is acknowledged with gratitude. The measurement of the cross-correlation was made with collaboration of Mr Y. Anezaki. The authors are grateful to Mr T. Sampo, Technical Officer, for his help in constructing the blunt circular cylinder employed in this study.

REFERENCES

Bar-Sever, A. 1989 Separation control on an airfoil by periodic forcing. *AIAA J.* **27**, 820–821.

Bhattacharjee, F. K., Scheelke, B. & Troutt, T. R. 1986 Modification of vortex interactions in a reattaching separated flow. *AIAA J.* **24**, 623–629.

Cherry, N. J., Hillier, R. & Latour, M. E. M. P. 1984 Unsteady measurements in a separated and reattaching flow. *J. Fluid Mech.* **144**, 13–46.

Cooper, P. I., Sheridan, J. C. & Flood, G. J. 1986 The effects of sound on forced convection over a flat plate. *Intl J. Heat Fluid Flow* **7**, 61–68.

Gad-el-Hak, M. & Bushnell, D. M. 1991 Separation control: Review. *Trans. ASME: J. Fluids Engng* **113**, 5–30.

Ho, C. M. & Huang, P. 1982 Subharmonics and vortex merging in mixing layers. *J. Fluid Mech.* **119**, 443–473.

Huang, L. S., Maestrello, L. & Bryant, T. D. 1987 Separation control over an airfoil at high angles of attack by sound emanating from the surface. *AIAA Paper* 87-1261.

Inoue, O. 1992 Double-frequency forcing on spatially growing mixing layers. *J. Fluid Mech.* **234**, 553–581.

Kelly, R. E. 1967 On the stability of an inviscid shear layer which is periodic in space and time. *J. Fluid Mech.* **7**, 657–689.

Kiya, M. 1989 Separation bubbles. In *Theoretical and Applied Mechanics* (ed. P. Germain, M. Piau & D. Caillerie), pp. 173–191. North-Holland.

Kiya, M., Mochizuki, O., Tamura, H., Nozawa, T., Ishikawa, R. & Kushioka, K. 1991 Turbulence properties of an axisymmetric separation-and-reattachment flow. *AIAA J.* **29**, 936–941.

Kiya, M. & Nozawa, T. 1987 Turbulence structure in the leading-edge separation zone of a blunt circular cylinder. *Trans. JSME* B **53**, 1183–1189 (in Japanese).

Kiya, M. & Sasaki, K. 1983 Structure of a turbulent separation bubble. *J. Fluid Mech.* **137**, 83–113.

Kiya, M., Shimizu, M., Mochizuki, O. & Ido, Y. 1993 Active forcing of an axisymmetric leading-edge turbulent separation bubble. *AIAA Paper* 93-3245.

Kiya, M., Shimizu, M., Mochizuki, O. & Ido, Y. 1995 Bimodal forcing of a turbulent leading-edge separation bubble. In *Separated and Complex Flows* (ed. M. V. Otugen, M. Kiya, J. C. Dutton, B. Reichert & G. C. Vradis). FED Vol. 217, pp. 175–182. ASME.

Nakamura, Y. & Nakashima, M. 1986 Vortex excitation of prisms with elongated rectangular, H and ⊢ cross sections. *J. Fluid Mech.* **163**, 149–169.

Nishioka, M., Arai, M. & Yoshida, S. 1990 Control of flow separation by acoustic excitation. *AIAA J.* **28**, 1909–1915.

Nishioka, M. & Morkovin, M. V. 1986 Boundary layer receptivity to unsteady pressure gradients: Experiments and overview. *J. Fluid Mech.* **171**, 219–261.

Parker, R. & Welsh, M. C. 1983 Effects of sound on flow separation from bluff flat plates. *Intl J. Heat Fluid Flow* **4**, 113–127.

Paschereit, C. O., Wygnanski, I. & Fiedler, H. E. 1995 Experimental investigation of subharmonic resonance in an axisymmetric jet. *J. Fluid Mech.* **283**, 365–407.

Raman, G. & Rice, E. J. 1989 Subharmonic and fundamental high amplitude excitation of an axisymmetric jet. *AIAA Paper* 89-0993.

Riley, J. J. & Metcalfe, R. W. 1980 Direct numerical simulation of a perturbed turbulent mixing layer. *AIAA Paper* 80-0274.

Roos, S. W. & Kegelman, J. T. 1986 Control of coherent structures in reattaching laminar and turbulent shear layers. *AIAA J.* **24**, 1956–1963.

https://doi.org/10.1017/S0022112097005521 Published online by Cambridge University Press

Roos, S. W. & Kegelman, J. T. 1987 Evolving three-dimensionality in a reattaching two-dimensional turbulent shear layer. *AIAA Paper* 87-1210.

Roshko, A. 1954 A new hodograph for free streamline theory. *NACA TN* 3168.

Roshko, A. 1955 On the wake and drag of bluff bodies. *J. Aero. Sci.* **22**, 124–132.

Ruderich, R. & Fernholz, H. H. 1986 An experimental investigation of a turbulent shear flow with separation, reverse flow, and reattachment. *J. Fluid Mech.* **163**, 283–322.

Shimizu, M., Kiya, M., Mochizuki, O. & Ido, Y. 1993 Response of an axisymmetric separation bubble to sinusoidal forcing. *Trans. JSME* B **59**, 721–727 (in Japanese).

Sigurdson, L. W. 1995 The structure and control of a turbulent reattaching flow. *J. Fluid Mech.* **298**, 139–165.

Sigurdson, L. W. & Roshko, A. 1988 The structure and control of a turbulent reattaching flow. In *Turbulence Management and Relaminarization* (ed. H. W. Liepmann & R. Narasimha), pp. 497–514. Springer.

Stokes, A. N. & Welsh, M. C. 1986 Flow-resonant sound interaction in a duct containing a plate, II: Square leading edge. *J. Sound Vib.* **104**, 55–73.

Sutton, E. P., Evans, G. P., McGuinness, M. D. & Svehla, K. M. 1981 Influence of wall vibrations on a flow with boundary-layer separation at a convex edge. In *Unsteady Turbulent Shear Flows* (ed. R. Michel, J. Cousteix & R. Houdeville), pp. 284–293. Springer.

Zaman, K. B. M. Q., Bar-Sever, A. & Mangalam, S. M. 1987 Effect of acoustic excitation on the flow over a low-*Re* airfoil. *J. Fluid Mech.* **182**, 127–148.

https://doi.org/10.1017/S0022112097005521 Published online by Cambridge University Press